Novel concepts to construct cost effective geothermal wells with Electro Pulse Power Technology

Initial heat production, well integrity modelling and cement strain-resistivity

Deliverable D5.2

The project DEEPLIGHT is subsidized through the GEOTHERMICA and JPP Smart Energy Systems Joint Call by Netherland Enterprise Agency, RVO, German Federal Ministry for Economic Affairs and Energy BMWi, Icelandic Research Institute, RANNIS, The Scientific and Technological Research Council of Turkey, TÜBİTAK, United States Department of Energy, DOE.

The contents of this publication reflect only the view of the author(s) and do not necessarily reflect the opinion of any of these funding agencies.

Review process

Project name	Novel concepts to construct cost effective geothermal wells with Electro Pulse Power Technology – "Deeplight"	
Funding scheme	Joint Call 2021 – GEOTHERMICA and JPP Smart Energy Systems	
Project no.	445	
Duration	01/11/2022 – 31/10/2025	
Work package	WP5 – Integrated Well-Integrity Approach for Electro-pulse Drilled Wells (LBNL)	
Dissemination level	Public	
Submission date	20/02/2025	
Due date	31/10/2024	
Author(s)	Jonny Rutqvist	
Contributors		
Verified (WP leader)	Jonny Rutqvist	Date: 08/11/2024
Approved (coordinator)	Jens Wollenweber	Date: 20/02/2025
Version	2.0	

Version history

Version	Publication date	Updates	Approved (coordinator)	Approval date
1.0	08/11/2025	Initial version	-	-
2.0	20/02/2025	Final review	Yes	20/02/2025

Executive summary

The overall aim of the DEEPLIGHT project is to accelerate the growth of global geothermal production by a game changing drilling and well construction system. One of the main objectives is to develop contactless drilling with Electro Pulse Power (EPP) technology along with a design for casing placement drilling as to be a game changer being far superior to conventional drilling methods. The objective of Work Package 5 (WP5) is to investigate thermal flexible, smart cement tailored to the requirements of the integrated EPP-casing while drilling approach. The novel drilling technology enables the optimization of wellbore sealing solutions using graphene-enhanced cements, optimizing electrical and elastic cement properties to maintain integrity during cyclic thermal loading and enabling self-sensing cement integrity monitoring concepts as an integral part of the new approach leading to higher reliability and prolonged life of the well. This deliverable report is generated for the project's WP5 on well integrity approach for EPP drilled wells focusing on Modelling Heat Production and Well Integrity.

This report presents the initial modeling of heat production and well integrity performed at Lawrence Berkeley National Laboratory (LBNL). A large diameter geothermal well model has been developed based on the linking of LBNL's T2Well simulator for multiphase fluid flow and heat transfer in wells with the FLAC3D mechanical simulator for well integrity. The model has been tested and demonstrated to be able to model geothermal production through a 3-km deep well, 0.5 m in diameter, along with well casing and cement mechanical responses. The model is currently being applied for initial modeling of heat production, well integrity modeling and cement strain–resistivity. At this stage, preliminary results of the model can be used to inform about the potential for the application of self-sensing cement in a geothermal well, including what are the temperature, pressure, stress and strain changes that can be expected. This may inform the selection of additives and guide laboratory the testing. The ongoing modeling include production from a hot steam reservoir, including assumed daily production cycles to investigate potent cyclic mechanical responses in the well cement.

From the preliminary results presented here, the potential for self-sensing has been indicated by relating calculated stress and strain changes to experimental observations of stress and strain induced resistivity changes. Moreover, the simulations clearly show the importance of the mechanical properties, i.e. cement deformability and strength that are properties that can be modified by additives considered in this study. Finally, the results indicate that current laboratory data in the literature can be difficult to apply for defining self-sensing properties to be applied in modeling of self-sensing in geothermal wells.

Contents

Abbreviations

CNF	Cement with carbon nanofibers
DFM	Drift-Flux-Model
EPP	Electro Pulse Power
TRL	Technology Readiness Level
THM	Thermo-Hydro-Mechanical
UDM	User-defined model

Tables

Figures

1.Introduction

This first chapter introduces the background and scope of this report.

1.1. Background

One of the main objectives of the DEEPLIGHT project is to develop contactless drilling with Electro Pulse Power (EPP) technology as to be a game changer being superior to conventional drilling methods. Within the DEEPLIGHT project different fields of research are combined to develop new technologies related to geothermal energy. These reach from the development of a new drill bit based on the Electro Pulse Power technology to a new borehole construction process. This construction process is based on a casing while drilling approach and expects to lead to improved wellbore stability, a faster drilling progress and superior cutting removal. As part of this research, Work Package 5 (WP5) is to investigate thermal flexible, smart cement tailored to the requirements of the integrated EPP-casing while drilling approach. The novel drilling technology enables the optimization of wellbore sealing solutions using graphene-enhanced cements, optimizing electrical and elastic cement properties to maintain integrity during cyclic thermal loading and enabling self-sensing cement integrity monitoring concepts as an integral part of the new approach leading to higher reliability and prolonged life of the well. Overall, a technology readiness level (TRL) 6 of this novel drilling technology is aimed for.

1.2. Scope

This deliverable report is generated for the project's WP5 on well integrity approach for EPP drilled wells on modeling of heat projection and well integrity. Initial modeling of heat production, well integrity and cement strain-resistivity has been completed. The parameters applied in this modeling are based on literature data. Once project specific laboratory data on cement properties are available, these will be incorporated to the modeling.

The report begins in Section 2 with the description of the approach and methodology, i.e. description of the numerical simulator applied for the modeling of heat production and well integrity. Then, in Section 3, the actual model simulation results are presented and discussed, including heat production modeling, well integrity modeling, as well as an initial attempt to estimate the cement resistivity changes due to calculated stress and strain changes. Finally, concluding remarks are provided in Section 4.

2. Methodology and Approach

The modeling of heat production, well integrity and cement strain-resistivity is realized by employing a simulator based on the coupling of a wellbore flow simulator (T2Well) with a geomechanical simulator (FLAC3D). T2Well is a numerical simulator that can accurately simulate fluid and heat flow in both wellbore and reservoir (Pan and Oldenburg, 2014) including complex two-phase flow phenomena such as condensation/evaporation, counter flow, and gas lifting, etc. FLAC3D is an advanced geomechanical simulator (Itasca, 2012) that has previously been linked to several of LBNL's TOUGH-family codes for modeling of coupled multiphase fluid flow and geomechanical processes (Rutqvist, 2011; 2017), including extensive applications to the high-temperature geothermal system at The Geysers geothermal field (Rutqvist et al., 2016, and references therein). Using T2Well linked with FLAC3D enables accurate modeling of multiphase flow processes within the wellbore and effects of wellbore pressure and temperature changes on well integrity (including casing and cement) as well as in surrounding rock.

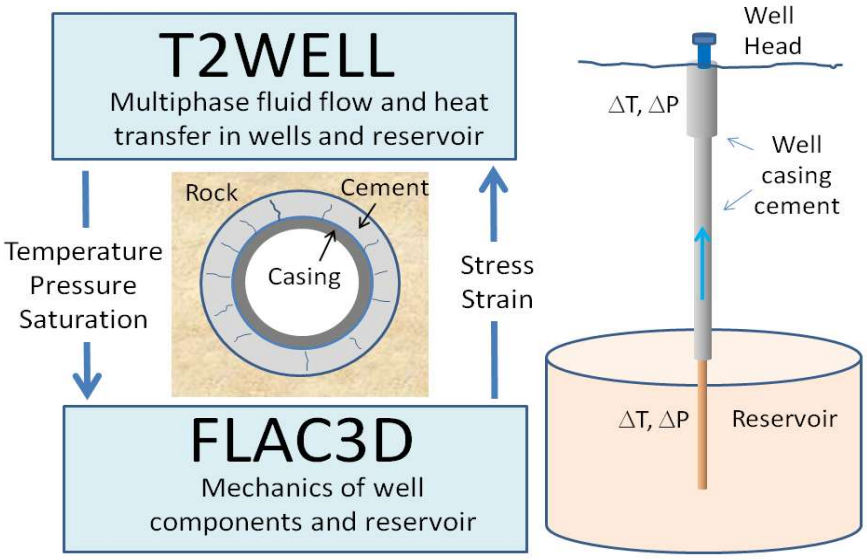

Figure 2-1. Coupling and interactions between T2Well for reservoir-wellbore multiphase flow and multicomponent transport modeling and FLAC3D for geomechanical modeling, with application to wellbore integrity analysis by including reservoir, wellbore and high +ΔT zone.

T2Well treats the wellbore–reservoir flow problem as an integrated system in which the wellbore and reservoir are two different subdomains where flow is controlled by the appropriate governing equations (1D two-phase momentum equation for the wellbore, and 3D multiphase Darcy's law for the reservoir). As a result, the governing equations for the flow processes in the wellbore–reservoir system are an extended set of those used by standard TOUGH2 (Table 2-1). As shown in Table 2-1, the major differences in governing equations between the wellbore and the reservoir are the definitions of energy flow terms and phase velocities. Because the velocities in the reservoir are usually very small, the kinetic energy can be ignored in the energy balance and the phase velocities can be calculated by the multiphase version of Darcy's law. However, this is not the case in the wellbore, where the kinetic energy cannot be ignored and the phase velocities are governed by the two-phase momentum equations. Even though the wellbore flow can be reasonably simplified as 1D, the two-phase momentum equations are still very difficult to solve mainly because of the complex and flow-rate-dependent two-phase flow structure in the wellbore. The Drift-Flux-Model (DFM), first developed by Zuber and Findlay (1965) and Wallis (1969), among others, provides an efficient way to approximate the complex two-phase flow in the wellbore (Pan and Oldenburg, 2014).

Table 2-1. The mass and energy balance equations solved in T2Well (Pan and Oldenburg, 2014)

Description		Equation
Conservation of mass and energy		$\frac{d}{dt}\int_{V_n} M^\kappa \, dV_n = \int_{\Gamma_n} \mathbf{F}^\kappa \bullet \mathbf{n} \, d\Gamma_n + \int_{V_n} q^\kappa \, dV_n$
Mass accumulation		$M^\kappa = \phi \sum_\beta S_\beta \rho_\beta X_\beta^\kappa$, for each mass component
Mass flux		$\mathbf{F}^\kappa = \sum_\beta X_\beta^\kappa \rho_\beta \mathbf{u}_\beta$, for each mass component
Porous media	Energy flux	$\mathbf{F}^\kappa = -\lambda \nabla T + \sum_\beta h_\beta \rho_\beta \mathbf{u}_\beta$
	Energy accumulation	$M^\kappa = (1-\varphi)\rho_R C_R T + \varphi \sum_\beta \rho_\beta S_\beta U_\beta$
	Phase velocity	$\mathbf{u}_\beta = -k \frac{k_{r\beta}}{\mu_\beta} (\nabla P_\beta - \rho_\beta \mathbf{g})$ Darcy's Law
Wellbore	Energy flux	$F^\kappa = -\lambda \frac{\partial T}{\partial z} - \frac{1}{A} \sum_\beta \frac{\partial}{\partial z} \left[A \rho_\beta S_\beta u_\beta \left(h_\beta + \frac{u_\beta^2}{2} + gz \cos\theta \right) \right] - q'$
	Energy accumulation	$M^\kappa = \sum_\beta \rho_\beta S_\beta \left(U_\beta + \frac{u_\beta^2}{2} + gz \cos\theta \right)$
	Phase velocity	$u_G = C_0 \frac{\rho_m}{\rho_m^*} u_m + \frac{\rho_L}{\rho_m^*} u_d$
		$u_L = \frac{(1-S_G C_0)\rho_m}{(1-S_G)\rho_m^*} u_m - \frac{S_G \rho_G}{(1-S_G)\rho_m^*} u_d$
		Drift-Flux-Model

2.1. FLAC3D Fundamentals

The FLAC3D code is developed for rock and soil mechanics and can also handle coupled thermomechanical and hydromechanical processes for single-phase fluid flow (Itasca, 2012). When running the FLAC3D code in its mechanical or thermomechanical configuration mode, it solves the equation of motion,

$$\nabla \cdot \boldsymbol{\sigma} + \rho_m \mathbf{g} = \rho_m \frac{d\mathbf{v}}{dt} \tag{2-1}$$

in an iterative manner with a stress-strain law. The incremental stress and strain during a time step is governed by various elastic or elasto-plastic constitutive laws, which can be written in a general form as

$$\Delta\sigma' = \mathbf{H}(\sigma', \dot{\varepsilon}\Delta t) \tag{2-2}$$

in which **H** contains given material functions, $\dot{\varepsilon}$ is the infinitesimal strain-rate tensor, and Δt is a time increment. The infinitesimal strain rate, $\dot{\varepsilon}$ and infinitesimal strain, **ε,** is governed by the restrictions

$$\dot{\varepsilon} = \frac{1}{2}(\nabla \mathbf{v} + (\nabla \mathbf{v})^{\mathrm{tr}}) \qquad \varepsilon = \frac{1}{2}(\nabla \mathbf{u} + (\nabla \mathbf{u})^{\mathrm{tr}}) \tag{2-3}$$

where tr denotes the transpose of a tensor. As usual, the total strain increment can be decomposed into elastic, plastic, and thermal expansion parts, according to:

$$\Delta\boldsymbol{\varepsilon} = \Delta\boldsymbol{\varepsilon}^e + \Delta\boldsymbol{\varepsilon}^p + \Delta\boldsymbol{\varepsilon}^T \tag{2-4}$$

where the thermal strain is given by

$$\Delta\boldsymbol{\varepsilon}^{T} = \mathbf{I}\beta_T \Delta T \tag{2-5}$$

where β_T is the linear thermal expansion coefficient, $\mathbf{I}$ is the unit tensor and T is the temperature.

The constitutive laws in Equation (2-2) work on the effective stress given by

$$\boldsymbol{\sigma}' = \boldsymbol{\sigma} + \mathbf{I}\alpha P \tag{2-6}$$

where α is Biot's effective stress parameter (Rutqvist, 2011) and P is pore pressure.

FLAC3D contains a number of structural elements (e.g. shells and liners) as well as an interface element that can be applicable to modeling a well assembly with multiple casings and cement sheaths. A large number of constitutive mechanical models are available for the modeling of the elasto-plastic behavior of rock, cement and steel, and if needed, a number of creep constitutive models. The models may also be modified using user-defined model (UDM) capabilities in FLAC3D. The frictional interface elements can be used to represent interfaces between cement and casing, for example, for modeling potential de-bounding. Frictional strength in the form of cohesion and internal friction angle defines the interface shear strength and a tensile cut-off can be defined with an interface tensile strength.

2.2. T2Well-FLAC3D Coupling Procedure

T2Well and FLAC3D are sequentially coupled, whereby fluid flow variables, such as pore pressure, temperature, and saturation calculated by T2Well, are transferred to a compatible numerical grid for FLAC3D, which then calculates effective stresses, thermal strains and associated deformations, returning updated values for porosity, permeability, and capillary strength parameter to T2Well. The sequential coupling technique was previously adopted for linking the TOUGH2 reservoir simulator to the FLAC3D geomechanics simulator (Rutqvist, 2011; 2017). The coupling scheme is based on the fixed stress-split sequential method (Kim et al., 2011). In this method, the flow problem is solved first (with an explicit evaluation of the volumetric total stress) and the pore pressure and the temperature are prescribed during the geomechanical calculation, which therefore requires drained mechanical properties.

In Figure 2-2, the data exchanges between T2Well and FLAC3D are illustrated with arrows going through the central THM model. The arrow on the right-hand side of Figure 2-2 shows the transmission of the effective stress σ' and strain ε (computed in FLAC3D) to T2Well for calculation of the updated porosity ϕ and the corresponding porosity change $\Delta\phi$. This mechanically induced $\Delta\phi$ has an immediate effect on fluid flow behavior. For example, if a change in σ' and ε causes ϕ to decrease, the pore pressure is expected to rise, especially if the permeability is low. The changes in porosity with effective stress can be calculated based on material specific laws. For example, an empirical model (proposed by Rutqvist et al., 2002) describes a nonlinear change in porosity ϕ as a function of the effective mean stress. Such a function could be applicable to both rock and cement and to update the permeability k. The updated ϕ and k values are in turn used to estimate changes in the hydraulic and wettability

properties of the porous medium (i.e., aqueous- and gas-phase relative permeabilities and capillary pressure P_c) by employing appropriate scaling equations.

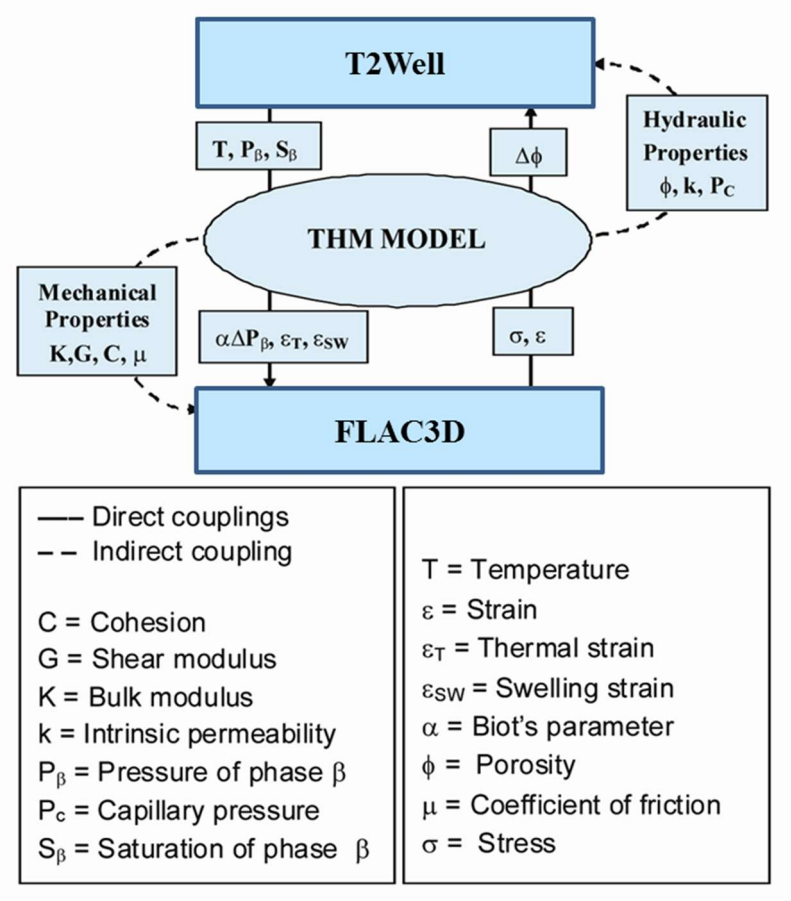

Figure 2-2. Schematic of linking T2Well and FLAC3D for coupled THM simulations of well integrity and reservoir behavior.

The arrow on the left side of Figure 2-2 depicts the flow of data obtained from T2Well (namely pressure P, temperature T, and phase saturations S_β) to FLAC3D for processing and estimates their impact on the effective stress $\alpha\Delta P_\beta$ (α being Biot's effective stress parameter), as well as on thermal and swelling strains (ε_T and ε_{sw}, respectively. Additionally, changes in P, T, and S_β may also result in changes in other mechanical properties, as listed in Figure 2-2. These include bulk modulus K, shear modulus G, cohesion C, and coefficient of internal friction μ.

One practical advantage with the sequential coupling technique adopted for T2Well-FLAC3D is the flexibility in the discretization of the problem domain for the thermal-hydraulic (T2Well) and mechanical (FLAC3D) analyses. In particular, the thermal-hydraulic analysis will require discretization of the entire well assembly and surrounding rock formations, while the mechanical analysis might be focused on different sections of the well. For example, the mechanical analysis may be focused on shallow regions of the well where the largest pressure and temperature changes could occur (Figure 2-1). Moreover, the flexibility in the mesh discretization enables inclusion of other critical mechanical components into the mechanical analysis of the well assembly, such as slip interfaces between cement and casing that may significantly impact the mechanical behavior within the well assembly. Cement resistivity changes are in this initial analysis be analyzed using empirical relationships between resistivity and stress or strain that can be found in the literature. In such analysis we will be able to model heat production along with stress, strain and resistivity changes in the well cement.

3. Geothermal Production Modeling and Well Integrity modeling with resistivity change

This section presents testing and demonstration of the applicability of the T2Well-FLAC3D modeling tool for the analysis of coupled THM processes and well integrity. We note that each of the individual codes T2Well and FLAC3D, have been extensively verified and validated (Pan and Oldenburg 2014; Itasca, 2012). Here we focus on some of the processes that are deemed most important for well integrity analysis and provide realistic full scale demonstration examples of geothermal wells. We first present T2Well thermal-hydraulic analyses of production from a geothermal well in steam-dominant geothermal systems. Thereafter, the fully coupled T2Well-FLAC3D results are presented along with initial results on cement strain-resistivity.

3.1. T2Well thermal hydraulic analysis

In this simulations, the conditions and properties from Geysers geothermal field in California was used to assure realistic field conditions in the model. The production data was from Prati 25 (P25), which is one of the production wells associated with an Enhanced Geothermal Systems (EGS) Demonstration Project that was conducted at the northwestern part of the Geysers (Rutqvist et al., 2016). The site is well characterized and extensively modeled related to reservoir pressure, temperature and properties and reservoir responses to liquid fluid injection (Rutqvist et al., 2016). The main steam reservoir (so-called normal temperature reservoir at The Geysers) typically has a reservoir temperature of about 240°C and a steam pressure on the order of a few MPa. The model for a typical liquid-dominant geothermal system was then developed by using the same model of the well assembly and geological layering, but with an assumed hydrostatic fluid pressure and fully saturated with liquid water.

Figure 3-1 presents the well design and geological formations discretized for the T2Well simulation. The model includes detailed discretization to explicitly represent the various casings and behind casing cement sections. Radially, the model extends 1 km, sufficiently far so that the outer boundary does not impact the simulation results around the well. Figure 3-2 shows the details of the model discretization outward to 1 m radius, at 3 different depths below the ground surface. T2Well integrates two simulation domains: the well and the surrounding formations. In the well, T2Well solves the 2-phase momentum equation using a so-called Drift-Flux Model (DFM) to obtain phase velocities, whereas in the surrounding formations, the multiphase Darcy's law is used for obtaining phase velocities (Pan and Oldenburg, 2014). The TOUGH2 fluid property module EOS1 is used in these simulations (Pruess et al., 2012). The pure water in its liquid, vapor, and two-phase states are calculated from steam table equations up to a temperature of 350°C, while vapor pressure lowering from capillary and adsorption effects is neglected. The initial thermal-hydrogeological conditions include linear gradients of pressure and temperature in the liquid-saturated overburden down to the top of the steam reservoir at about 1500 m depth. The pressure gradient in the overburden corresponds to hydrostatic pressure, whereas the temperature increases from about 25°C at the ground surface to about 250°C at 1500 m depth. In the steam reservoir (below 1500 m), the steam pressure is as low as about 3 MPa, whereas the temperature is around 250 to 260°C down to 3500 m depth. In the modeling presented here we assumed a constant boundary (1 atm and 25.46°C) at the ground surface except at the wellhead, whereas at the bottom of the model (3500 m depth), the pressure and temperature were held constant at 2.94 MPa and 265°C. An initial simulation was conducted using a steady production rate with comparison of P25 well production data on production rate, well head pressure and temperature to assure realistic field conditions. The result of this initial simulation with comparison to field data is shown in Figure 3-3. The T2Well

hydraulic and thermal material parameters are presented in Table 3-2. This includes formations, cement and steel casings.

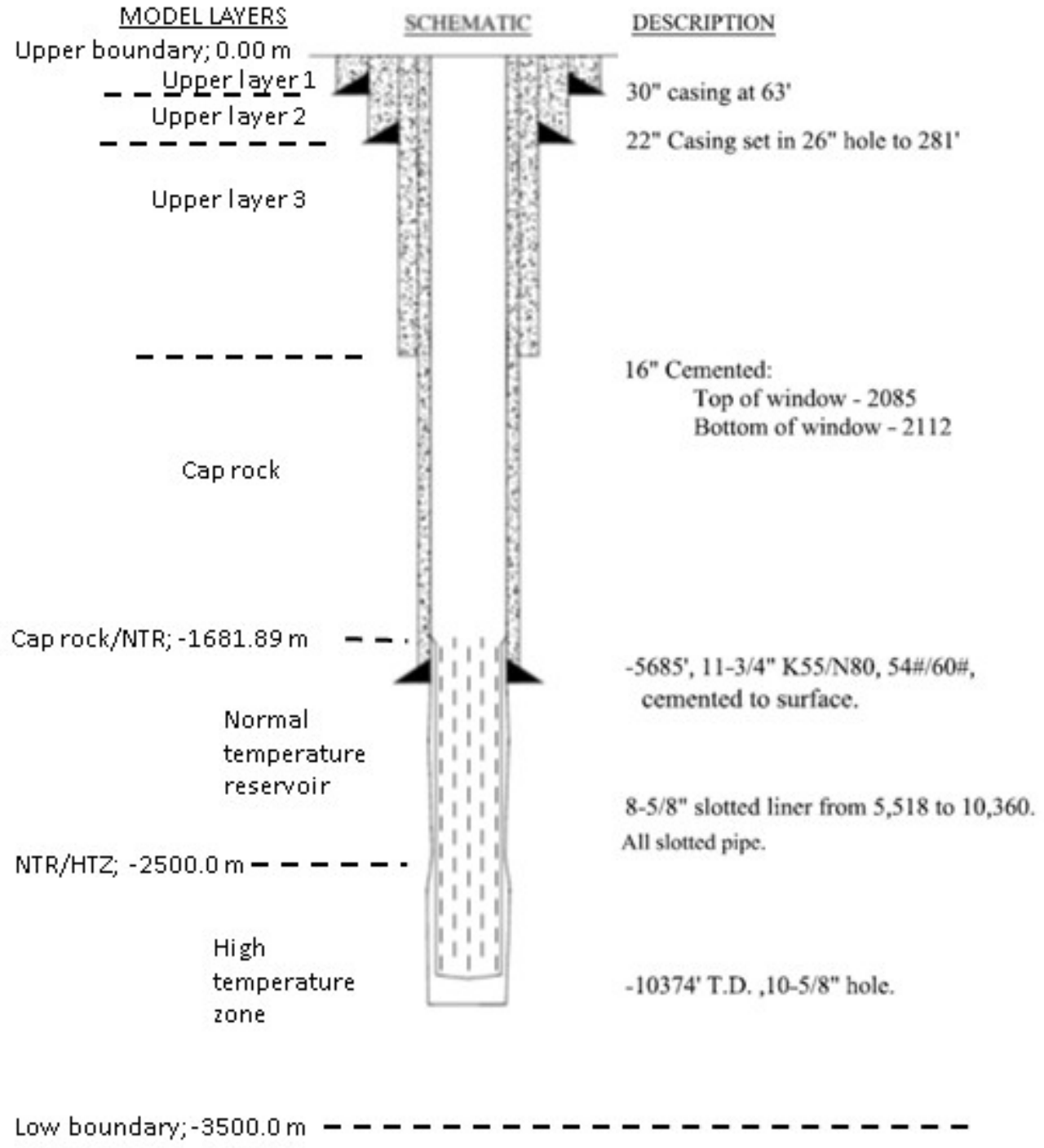

Figure 3-1. P25 well design at the Northwest Geysers and model layers used in T2Well for simulation of steady and variable geothermal production.

Table 3-1. Preliminary TH material parameters for T2Well simulations.

Name	Depth (m)	Porosity	Lateral permeability (m^2)	Vertical permeability (m^2)	Pore compressibility (Pa^{-1})	Heat conductivity (W/m^oC)	Specific heat (J/kg^oC)	Solid density (kg/m^3)	Maximum capillary pressure (Pa)
NTZhf	2500.0-3500.0	0.010	$2X10^{-14}$	$2X10^{-14}$	1.0E-10	3.20	1000.0	2700.0	10^5
NTRgw	1681.9-2500.0	0.015	$5X10^{-14}$	$5X10^{-14}$					
Caprk	643.7-1681.9	0.14	10^{-18}	10^{-18}		2.50			10^7
Capr0	85.6-643.7	0.24	10^{-18}	10^{-18}					
Capr1	19.2-85.6	0.34	10^{-16}	10^{-16}					
capr2	0-19.2	0.40	10^{-15}	10^{-15}					
poros	Borehole outside liner including rock within 11-3/4 inch	0.9016	10^{-12}	$5X10^{-10}$		3.20	1000.0		10^3
cemnt	Cement outside each casing	0.30	$2X10^{-18}$	$2X10^{-18}$		0.6	2116.4		10^7
steel	Wall of casing	0.00	0.0	0.0	0.0	43.0	473.0		0

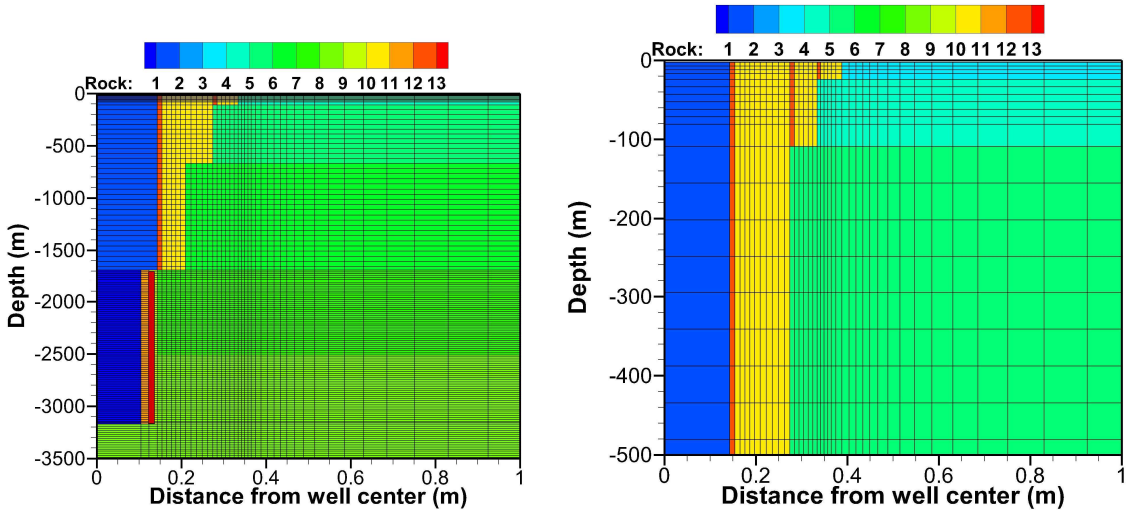

(a) (b)

Figure 3-2. Details of model discretization to 1 m radius from the center of the well. (a) Mesh discretization from 0 to 3500 m depth and (b) details of the upper 500 m of the well and surrounding rock.

The simulations were conducted by first modeling steady production for 100 days to obtain quasi- steady-state conditions of temperature in the well assembly and surrounding geological formations.

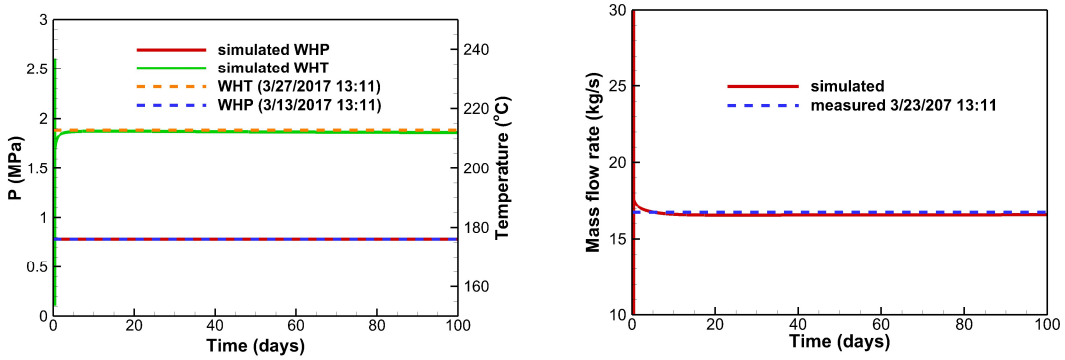

(a) (b)

Figure 3-3. Evolution of (a) pressure and (b) mass flow rate with comparison of simulation and measurements.

3.2. T2Well-FLAC3D well integrity analysis

The approach taken here is to develop a 3D mechanical model for perhaps one of the most vulnerable parts of the well assembly in this context, namely its shallowest part. Figure 3-4 shows the 3D mechanical model of the well assembly and how it is linked to the larger scale T2Well simulation model.

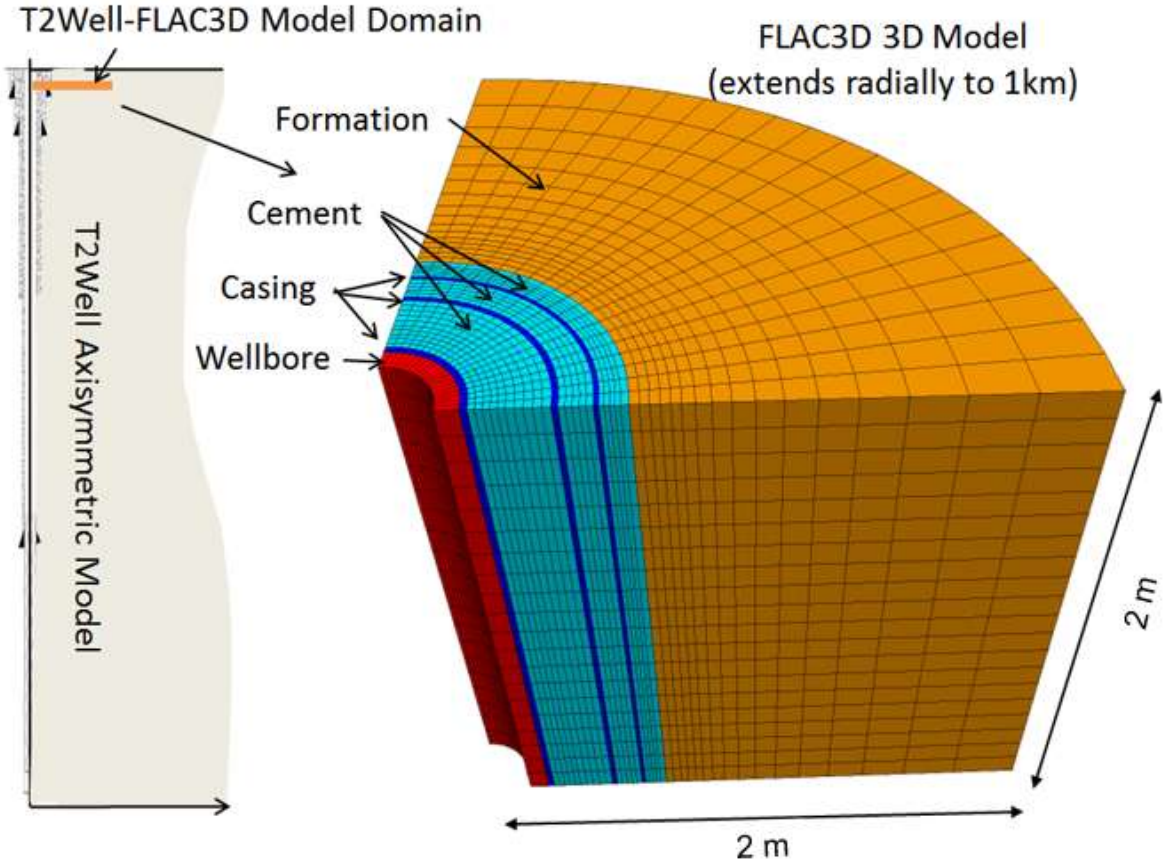

Figure 3-4. Coupled T2Well and FLAC3D model domains, including T2Well large scale axial symmetric model domain and FLAC3D mechanical model domain of the shallowest part of the production well.

Again, the flexibility of the sequential coupling between T2Well and FLAC3D makes it possible to conduct the coupled T2Well-FLAC3D THM analysis for each component of the system, whereas other parts are solved only for TH processes using the T2Well.

As described above, the T2Well simulations were conducted using an axisymmetric model domain, but the T2Well-FLAC3D coupled THM analysis is conducted on co-located numerical grid elements. This means that the pressure and temperature evolution calculated in T2Well at a depth of 2.4 m is imported into the mechanical analysis along the radius of the 3D model. In this particular case, a large diameter geothermal well model was considered by increasing the diameter to 0.5 m at 3 km depth.

The main reason for adopting a 3D model in the mechanical analysis is the desire to be able to apply anisotropic horizontal in situ stress. In this particular case at 2.4 m depth, the in situ stresses are very small and there would not be much of mechanical force from the surrounding formations on the well assembly at this depth. However, if performing similar well integrity analysis at depth, the in situ stress field could have a significant impact, including forcing and providing mechanical confinement. The mechanical model includes components of host rock, cement and casings as well as slip interfaces between these components. These slip interfaces allow for frictional failure using Coulomb criterion as well as elastic opening of the interfaces or breaking up by tensile failure.

Figure 3-5 shows the evolution of temperature and fluid pressure in the cement between the two outermost casings. As shown, the temperature increases in several days and this creates pressure changes through thermal pressurization. These temperature and pressure changes in turn causes significant mechanical changes in the well assembly. The mechanical responses are calculated considering elasto-plastic properties of the cement, rock and frictional interfaces (Table 3-2).

Table 3-2. Mechanical properties used in FLAC3D for modeling mechanical responses of the well assembly

Property	Material			
	Steel Casing	Cement	Formation	Interfaces
Young's modulus, E (GPa)	200	10	5	NA
Poisson's ratio, ν (-)	0.3	0.3	0.3	NA
Thermal expansion coefficient ($°C^{-1}$)	1.3×10^{-5}	1.0×10^{-5}	1.0×10^{-5}	NA
Friction angle, ϕ (-)	NA	20	10	20
Cohesion, *C*, (MPa)	NA	5.0	3.0	1.0
Tensile strength (MPa)	NA	3.0	1.0	0.0

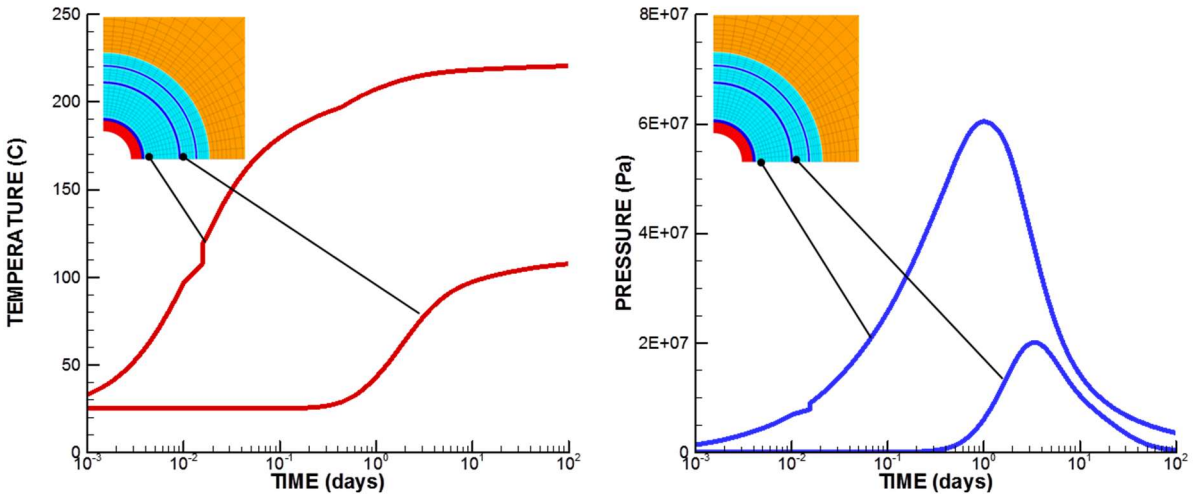

(a) (b)

Figure 3-5. Calculated (a) temperature and (b) pressure evolutions in two cement sections at the shallow part of the production well.

Figure 3-6 presents contours of temperature and pressure at after 2 days of production. This is at the time when temperature already has increased substantially in the inner parts of the well assembly and when the fluid pressure in the cement has reached a peak (Figure 3-5). We observe a sharp thermal gradient as well as a high pressure buildup on the two innermost cement sections that are located between steel casings. The high temperature increase and the pressure increase causes expansion of the innermost cement, expanding the entire well assembly radially and thereby creating forces on the outer parts of the well assembly. The surrounding formations, representing very shallow sediments, are very soft and do not provide much resistance of confinement for the well assembly.

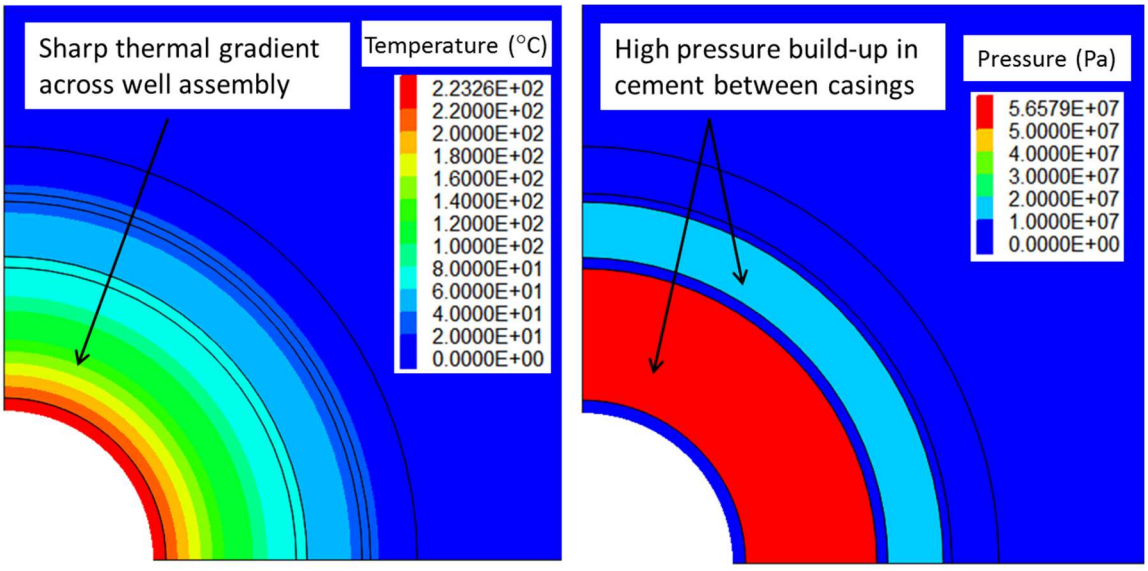

(a) (b)

Figure 3-6. Calculated (a) temperature and (b) fluid pressure distribution after 2 days of production.

Contours of maximum and minimum effective principal stresses are presented in Figure 3.7. Figure 3-7a shows that the expansion of inner parts of the well assembly results in tensile stress and tensile failure of the outer cement sections. Here we assumed a tensile strength of the

cement of 3 MPa. The surrounding sediment is very soft and has also reached its tensile strength of 1 MPa. At the same time, high compressive stresses are induced in the cement, just behind the innermost casing (Figure 3-7b). These high compressive stresses are caused by thermal stress, which here develops in the tangential direction and this results in a compressive shear failure that is limited in extent to the innermost cement.

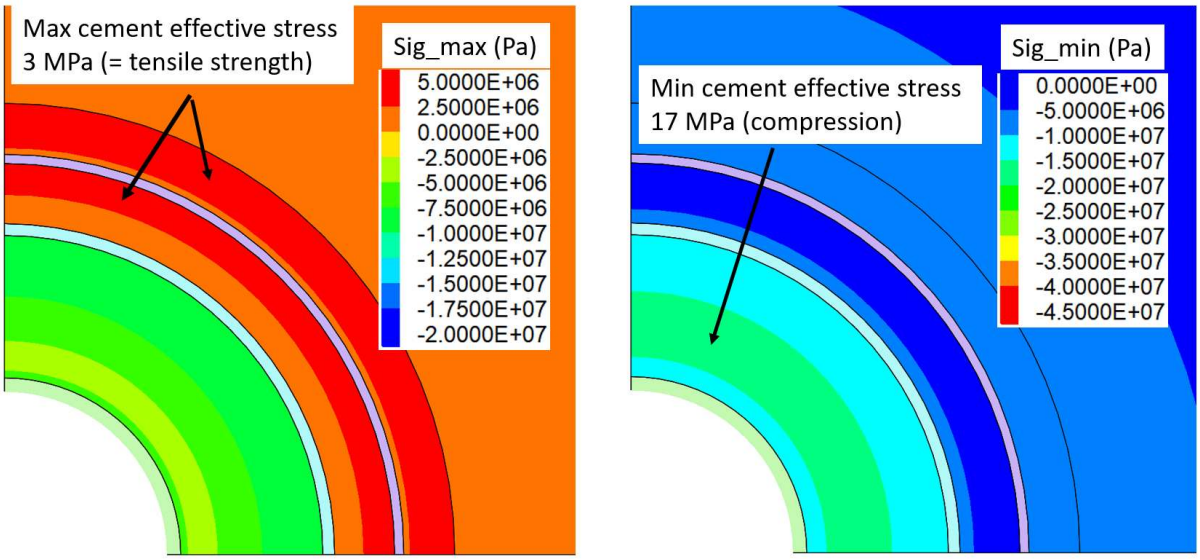

Figure 3-7. Calculated principal stress distributions in the cement and rock formations after 2 days of production (sign convention with tensile stress being positive): (a) Maximum principal effective stress and (b) minimum principal stress.

Figure 3-8 presents results of volumetric and shear strain in the cement. The inner cement is expanding caused by thermal expansion and thermal pressurization. The expansion near the inner casing is the largest with volumetric strain exceeding 3% (Figure 3.8a) The entire inner cement experience a volumetric strain of close to 1% or higher. Shear strain are also the highest at the same locations (Figure 3.8b).

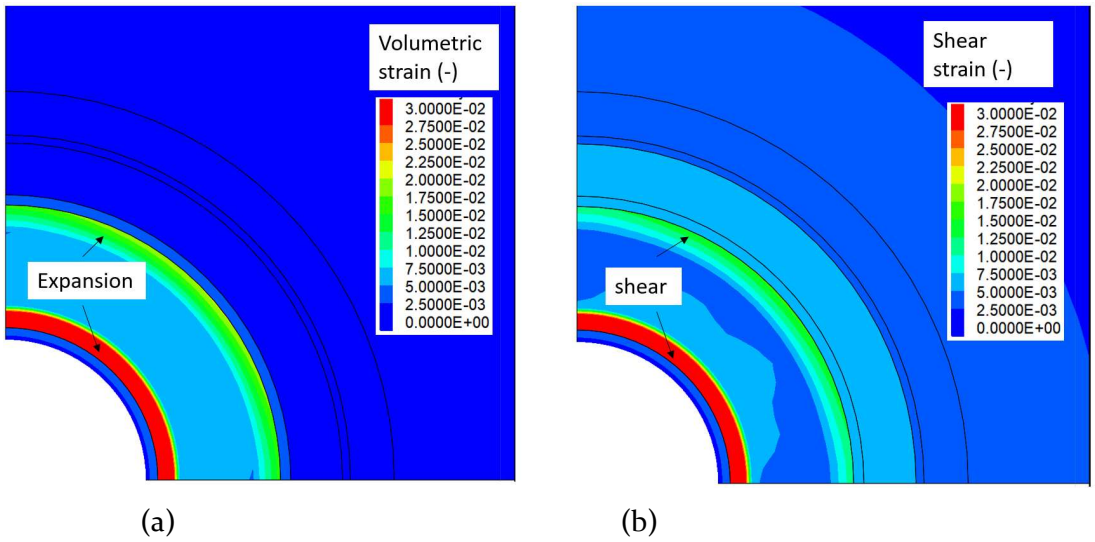

Figure 3-8. Calculated strain in the cement and rock formations after 2 days of production (sign convention expansion being positive): (a) Volumetric strain and (b) shear strain.

Figure 3-9 shows the stress path (maximum compressive versus minimum compressive stresses) in the 2nd cement section, with the Mohr-Coulomb failure envelope. It is shows that the stress evolution is very complex and that both tensile and shear yielding occur during the first few days of production. Thereafter, the principal stresses moves away from the failure line as a result of increasing thermal stress that provides an increasing confining stress.

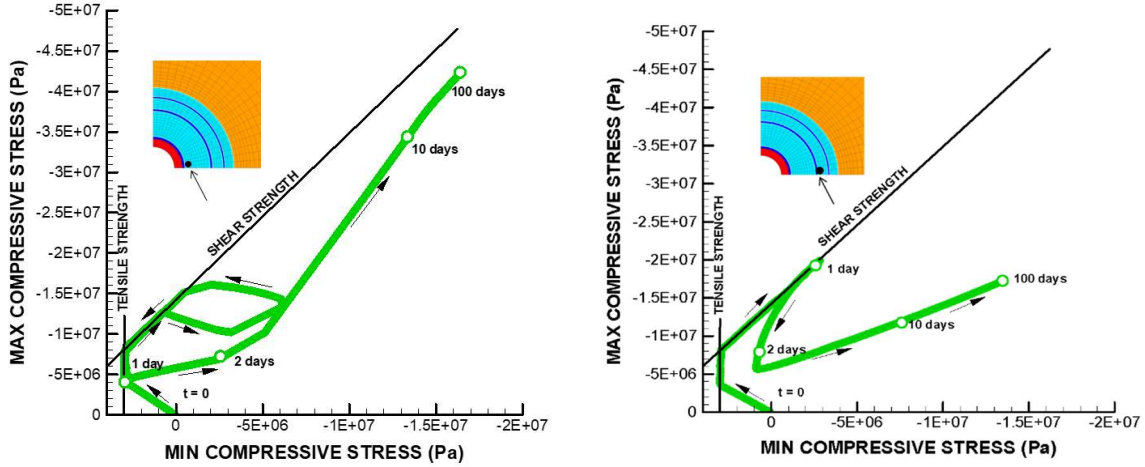

Figure 3-9. Effective stress path for locations behind casing in (a) the 1st cement and (b) the 2nd cement.

Figure 3-10 through 3-12 show the distribution of different stress components after 2 and 100 days of production, as well as for a case when temperature and fluid pressure has been returned to what they were initially, before the start of heat production. This will then show irreversible mechanical changes caused by the cement failure. In general, the results show the very strong and complex stress evolution during production with very high compressive stress developed towards the end of the 100 days production. Such high compressive stress can develop because of thermal stresses that provides confining stress. Highest shear stresses are developed in the first cement at the end of production at 100 days. The shear stresses are then relieved significantly after temperature and pressure returned to ambient. However, significant permanent shear stress remains with a magnitude of about 7 MPa in the first cement.

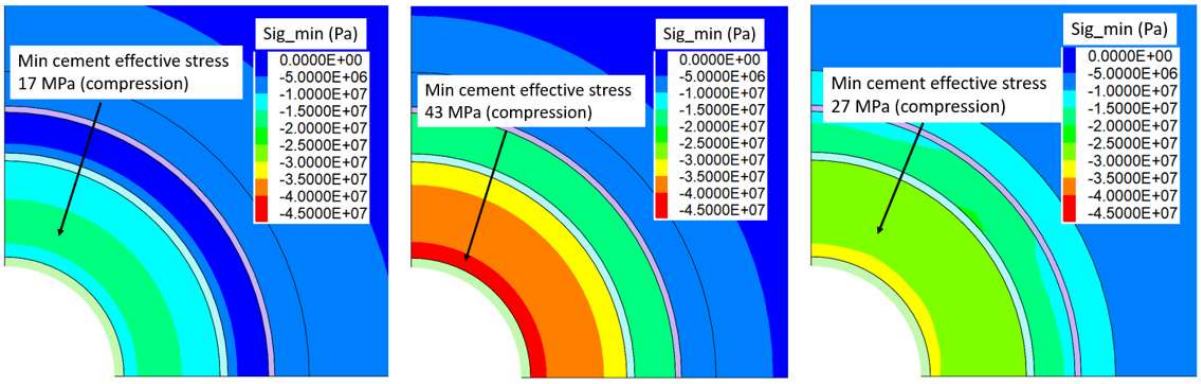

Figure 3-10. Calculated minimum principal stress distributions in the cement and rock formations after (a) 2 days of production, (b) 100 days of production, and (c) return to initial pressure and temperature conditions.

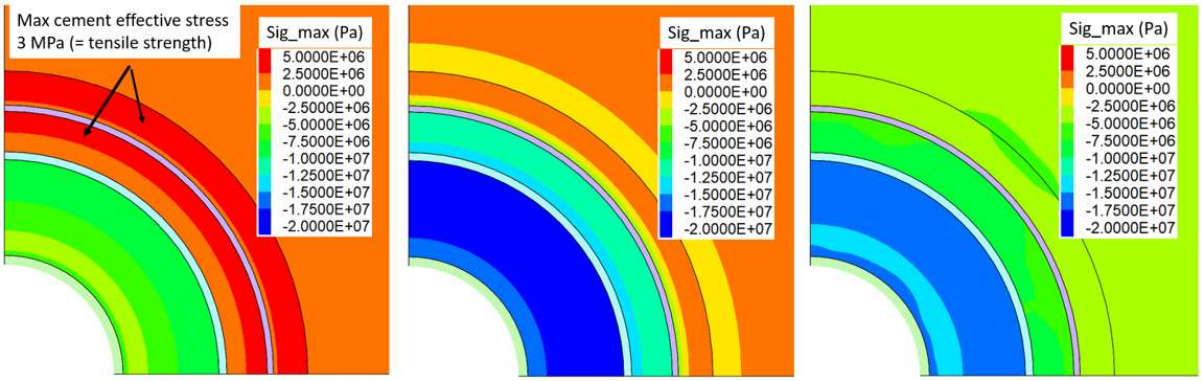

Figure 3-11. Calculated maximum principal stress distributions in the cement and rock formations after (a) 2 days of production, (b) 100 days of production, and (c) return to initial pressure and temperature conditions.

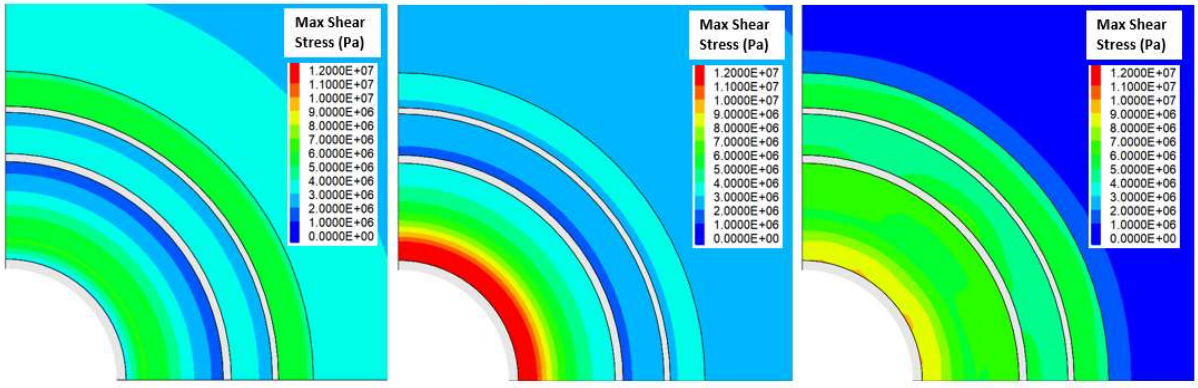

Figure 3-12. Calculated maximum shear stress distributions in the cement and rock formations after (a) 2 days of production, (b) 100 days of production, and (c) return to initial pressure and temperature conditions.

Figure 3-13 and 3-14 show the distribution volumetric and shear strains, respectively. In general, the largest strains are induced in the early time in the first cement section, at its innermost and outermost parts. Most of this strain seems to be induced by the mechanical failure causing irreversible strain. There is also some irreversible shear strain occurring in most cement parts of the well assembly.

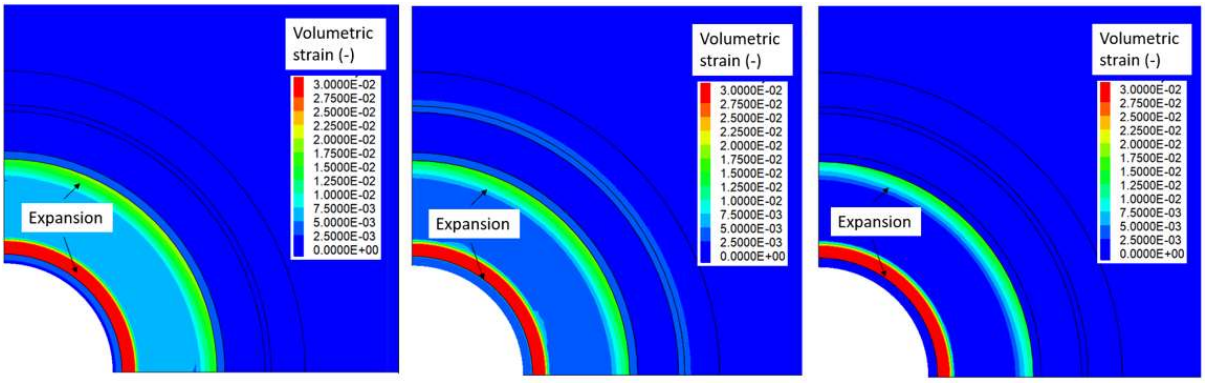

Figure 3-13. Calculated volumetric strain distributions in the cement and rock formations after (a) 2 days of production, (b) 100 days of production, and (c) return to initial pressure and temperature conditions.

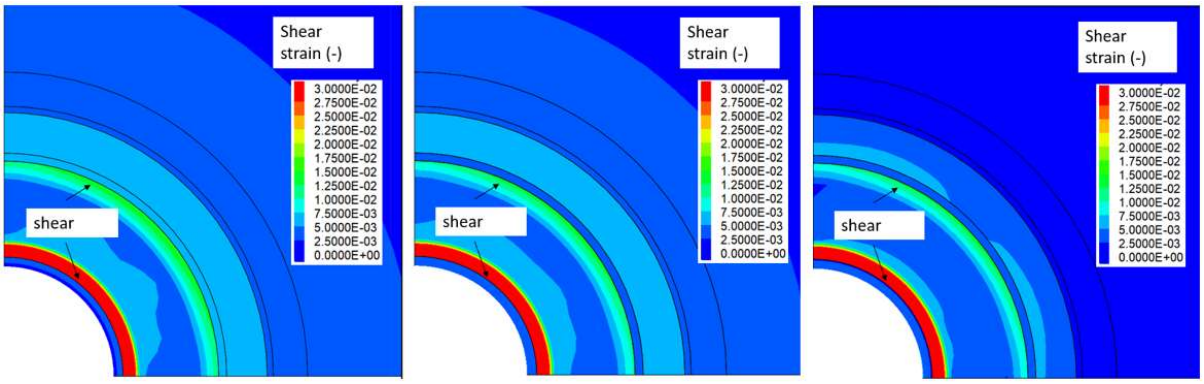

Figure 3-14. Calculated shear strain distributions in the cement and rock formations after (a) 2 days of production, (b) 100 days of production, and (c) return to initial pressure and temperature conditions.

3.3. Estimating resistivity changes

For the self-sensing potential, we may relate the obtained stress and strain changes with potential changes in resistivity as reported from experiments in the literature. For example, Gawel et al (2021), measured resistivity of Portland G—oil and gas well cement with carbon nanofibers (CNF) to axial load during uniaxial compressive strength test. The experiments showed fractional resistivity changes ranging from 50% - 150% when loading the samples through compressive failure. That is, the samples were loaded in uniaxial compression to a peak compressive stress of about 14 MPa and with axial strain about 3% at failure. This is similar somewhat similar to the stress and strain evolution in the simulation results with the results in Figures 3-9 to 3-12, but the loading path is quite different. The failure in the modeling is in parts of the model dominated by an initial tensile failure that then transfer into a shear failure. The initial tensile failure also leads to strain expansion rather than contraction. Therefore, it is not clear how to relate the calculated and stress and strain to those in compression experiments.

In another study, Wen and Chung (2007), presents experimental results of carbon fiber reinforced cement showing up to 40% fractional resistivity change associated with irreversible strain on the order of 1×10^{-4}. In the modeling here the irreversible strain is much larger than that and this would indicated significant changes in resistivity.

Vipulanandan (2022) presents results of uniaxial compression of piezoresistive cement samples after various curing times from 1 to 365 days. After 28 days, the samples could be loaded to a peak compressive stress of about 25 to 30 MPa, at which the resistivity fraction changes measured along the axial loading direction was about 100%.

It is difficult to relate the stress and strain sensitivity of all these uniaxial laboratory experiments to the stress and strain results from our well integrity modeling. Figure 3-15 shows one example where the changes in resistivity has been estimated from the distribution in maximum shear stress and volumetric strain. This has been achieved by simple linear relations between resistivity change and stress as well as between resistivity change and strain. The results with either method shows the most significant changes in resistivity at the innermost parts of the first cement section, just behind the first casing. However, the distribution of resistivity changes are quite different depending on if relating the resistivity changes to shear stress or volumetric strain. Based on these results one can conclude that more laboratory data is needed that better represent the conditions that can occur in a geothermal well assembly.

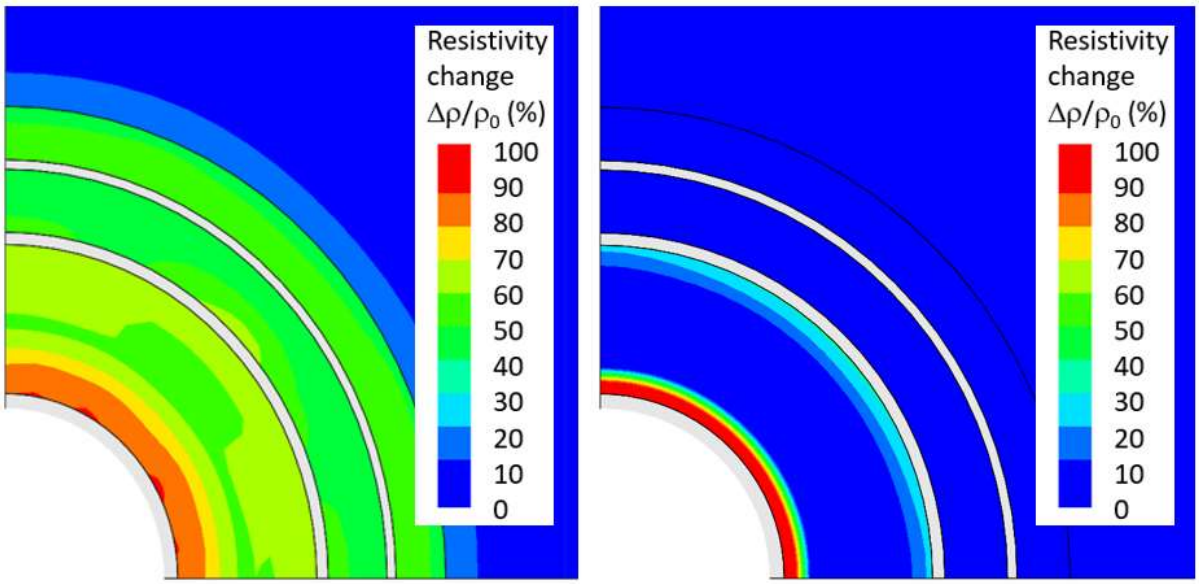

(a) (b)

Figure 3-15. Estimated resistivity change for the irreversible mechanical changes in the well assemble considering (a) stress sensitivity of resistivity or (b) strain sensitivity.

4. Concluding remarks

A large diameter geothermal well model has been developed based on the linking of LBNL's T2Well simulator for multiphase fluid flow and heat transfer in wells with the FLAC3D mechanical simulator for well integrity. At this stage, preliminary results of the model can be used to inform about the potential for the application of self-sensing cement in a geothermal well, including what are the temperature, pressure, stress and strain changes that can be expected. This may inform the selection of additives and guide laboratory the testing. The ongoing modeling include production from a hot steam reservoir, including assumed daily production cycles to investigate potent cyclic mechanical responses in the well cement. Preliminary results are stated as follows:

- The biggest risk of mechanical cement failure occurs during the initial start-up of production because of a large and rapid temperature increase from an initially cool temperature near the ground surface.
- During variable production with assumed daily production cycles, temperature fluctuations also result in fluctuations in pore pressure and stress with a relatively larger impact when producing from a very hot steam-dominated system.
- Both tensile and compressive cement failure can occur as a results temperature increase and thermal pressurization as a result the thermal expansion of fluids trapped in the cement.
- Key mechanical parameters for the stress and strain evolution in the cement are Young's modulus and cement strength, including compressive strength and tensile strength.

The current available laboratory data on self-sensing cement and resistivity changes are still quite scares and may not easily be applied to the mechanical evolution of geothermal well cement. Tests that better mimic the stress and strain evolution during thermal loading of a well assembly, e.g. cement between two steel casings would be desirable.

5. References

Itasca Consulting Group, 2012. FLAC3D, Fast Lagrangian Analysis of Continua in 3 Dimensions, Version 5.0, Minneapolis, Minnesota, Itasca Consulting Group.

Gawel, K., Szewczyk, D., and Cerasi, P.R., 2021. Self-sensing well cement. Materials, 14, 1235.

Kim, J., Tchelepi, H.A., and Juanes, R., 2011. Stability and convergence of sequential methods for coupled flow and geomechanics: Fixed-stress and fixed-strain splits. Computer Methods in Applied Mechanics and Engineering, (13-16), 1591-1606.

Pan, L., and Oldenburg, C., 2014. T2Well—An integrated wellbore–reservoir simulator. Computers & Geosciences 65, 46-55.

Pruess, K., Oldenburg, C., and Moridis, G., 2012. TOUGH2 User's Guide, Version 2.1, LBNL-43134, Lawrence Berkeley National Laboratory, Berkeley, California.

Rutqvist, J., 2011. Status of the TOUGH-FLAC Simulator and Recent Applications Related to Coupled Fluid Flow and Crustal Deformations. Computers & Geosciences, 37, 739–750.

Rutqvist, J., 2017. An overview of TOUGH-based geomechanics models. Computers & Geosciences, 108, 56–63.

Rutqvist, J., Wu, Y.-S., Tsang, C.-F. and Bodvarsson G.A., 2002. Modeling approach for analysis of coupled multiphase fluid flow, heat transfer, and deformation in fractured porous rock. International Journal of Rock Mechanics and Mining Sciences, 39, 429-442.

Rutqvist, J., Jeanne, P., Dobson, P. F., Garcia, J., Hartline, C., Hutchings, L., Singh, A., Vasco, D.W., and Walters, M., 2016. The Northwest Geysers EGS Demonstration Project, California - Part 2: Modeling and interpretation. Geothermics, 63, 120–138.

Vipulanandan, C., 2022. Smart cement: Development, testing, modeling and real-time monitoring. CRC Presss.

Wallis, G. B. (1969). One-Dimensional Two-Phase Flow. McGraw-Hill Book Company, New York.

Wen, S. and Chung, D.D.L., 2007. Electrical-resistance-based damage self-sensing in carbon fiber reinforced cement. Piezoelectric cement-based materials with large coupling and voltage coefficients. Carbon, 45, 710-716.

Zuber, N., Findlay, J.A. (1965). Average volumetric concentration in two-phase flow systems. Journal of Heat Transfer ASME 87 (4), 453–468.